



Frequency specific spatial interactions in human electrocorticography: V1 alpha oscillations reflect surround suppression

B.M. Harvey ^{a,*}, M.J. Vansteensel ^b, C.H. Ferrier ^b, N. Petridou ^c, W. Zuiderbaan ^a, E.J. Aarnoutse ^b, M.G. Bleichner ^b, H.C. Dijkerman ^{a,b}, M.J.E. van Zandvoort ^{a,b}, F.S.S. Leijten ^b, N.F. Ramsey ^b, S.O. Dumoulin ^a

^a Experimental Psychology, Helmholtz Institute, Utrecht University, Utrecht, 3584 CS, Netherlands

^b Department of Neurology and Neurosurgery, Rudolf Magnus Institute of Neuroscience, University Medical Center Utrecht, Utrecht, 3584 CX, Netherlands

^c Department of Radiology, Rudolf Magnus Institute of Neuroscience, University Medical Center Utrecht, Utrecht, 3584 CX, Netherlands

ARTICLE INFO

Article history:

Accepted 12 October 2012

Available online 18 October 2012

Keywords:

Electrocorticography
Alpha oscillation
Surround suppression
Broadband power
Population receptive field

ABSTRACT

Electrical brain signals are often decomposed into frequency ranges that are implicated in different functions. Using subdural electrocorticography (ECoG, intracranial EEG) and functional magnetic resonance imaging (fMRI), we measured frequency spectra and BOLD responses in primary visual cortex (V1) and intraparietal sulcus (IPS). In V1 and IPS, 30–120 Hz (gamma, broadband) oscillations allowed population receptive field (pRF) reconstruction comparable to fMRI estimates. Lower frequencies, however, responded very differently in V1 and IPS. In V1, broadband activity extends down to 3 Hz. In the 4–7 Hz (theta) and 18–30 Hz (beta) ranges broadband activity increases power during stimulation within the pRF. However, V1 9–12 Hz (alpha) frequency oscillations showed a different time course. The broadband power here is exceeded by a frequency-specific power increase during stimulation of the area outside the pRF. As such, V1 alpha oscillations reflected surround suppression of the pRF, much like negative fMRI responses. They were consequently highly localized, depending on stimulus and pRF position, and independent between nearby electrodes. In IPS, all 3–25 Hz oscillations were strongest during baseline recording and correlated between nearby electrodes, consistent with large-scale disengagement. These findings demonstrate V1 alpha oscillations result from locally active functional processes and relate these alpha oscillations to negative fMRI signals. They highlight that similar oscillations in different areas reflect processes with different functional roles. However, both of these roles of alpha seem to reflect suppression of spiking activity.

© 2012 Elsevier Inc. All rights reserved.

Introduction

Electrical signals arising from synchronized human neural activity are characterized by components oscillating at different frequencies, associated with different aspects of neural processing. This oscillatory activity can result from cyclical interactions of excitatory and inhibitory pools of neurons, but this general description typically covers a large range of possible neural mechanisms (Ermentrout and Kopell, 1998; Jones et al., 2000; Kopell et al., 2000; Traub et al., 1996).

In particular, 9–12 Hz (alpha) oscillations, commonly recorded using electro- and magneto-encephalography (EEG and MEG), may be involved in functionally important computations within the local neural

population (Cooper et al., 2003, 2006; Jensen and Mazaheri, 2010; Palva et al., 2005a, 2005b) or may simply reflect large-scale disengagement of task-irrelevant areas (Klimesch, 1996; Klimesch et al., 2007; Pfurtscheller, 2001, 2003; Ray and Cole, 1985). Computations within the local neural population suggest interactions with local neurons, while large-scale disengagement is likely to involve interactions with an inhibitory population in another part of the brain. Distinguishing between these possibilities is hindered by the low spatial resolution of recordings made outside the skull using EEG and MEG.

Here, we measure responses to visual stimuli using fMRI and electrocorticography (ECoG, intracranial EEG) in the same human subject. Both techniques have higher spatial resolution than EEG and MEG, and as such allow measurement of the aggregate neuronal receptive field within each recording site, the population receptive field (pRF) (Dumoulin and Wandell, 2008; Yeshor et al., 2007). We use pRF analysis to determine which stimulus positions elicit responses at the recording site. In early visual cortex, visual stimulation of areas outside the preferred visual field position of the neural population within an fMRI voxel causes decreases in BOLD fMRI signals (Logothetis, 2002; Tajima et al., 2010; Williams et al., 2003; Zenger-Landolt and Heeger, 2003), known as negative BOLD responses (NBR). The NBR are of

* Corresponding author at: Experimental Psychology, Helmholtz Institute, Utrecht University, Heidelberglaan 2, Utrecht, 3584 CS, Netherlands.

E-mail addresses: b.m.harvey@uu.nl (B.M. Harvey), m.j.vansteensel@umcutrecht.nl (M.J. Vansteensel), cferrier@umcutrecht.nl (C.H. Ferrier), n.petridou@umcutrecht.nl (N. Petridou), w.zuiderbaan@uu.nl (W. Zuiderbaan), e.j.aarnoutse@umcutrecht.nl (E.J. Aarnoutse), m.g.bleichner@umcutrecht.nl (M.G. Bleichner), c.dijkerman@uu.nl (H.C. Dijkerman), m.vanzandvoort@uu.nl (M.J.E. van Zandvoort), f.s.s.leijten@umcutrecht.nl (F.S.S. Leijten), nramsey@umcutrecht.nl (N.F. Ramsey), s.o.dumoulin@uu.nl (S.O. Dumoulin).

neural origin (Shmuel et al., 2006; Smith et al., 2004a). Recently, we extended the pRF model to include suppressive surrounds that capture the NBR (Zuiderbaan et al., 2012). The pRF surround influences signals at the recording site comparably to the suppressive surround of classical RF responses seen in electrophysiology (Carandini, 2004; Cavanaugh et al., 2002; Fitzpatrick, 2000).

We demonstrate that measurements of neural oscillations show a clear signature of surround suppression at alpha frequencies in V1 in the absence of classical receptive field stimulation. This process is likely to be a major source of alpha activity measured on the scalp near the occipital pole. The high spatial resolution of ECoG allows us to measure the local components of this activity, and demonstrate that it is tightly localized. Low frequency oscillations in IPS, including alpha, are more broadband and less local, suggesting that they result from a different process, such as inter-area large-scale disengagement.

Materials and methods

Subject information

The subject was a right-handed 20-year-old man with medically intractable seizures for 5 years. The subject had an aura of right hand tingling and showed speech arrest during seizures. MRI and FDG-PET were negative. Ictal EEG suggested a left-sided seizure onset in the parieto-temporo-occipital area. Because of the negative imaging results and the close relation to Wernicke's area, he underwent a subdural implantation of electrode grids covering the area. The clinical implantation scheme included placement of electrodes to sample from more posterior areas, including IPS and V1.

All candidates for subdural implantation undergo preoperative fMRI for clinical purposes and are asked to participate in ancillary scientific studies that include visual tests during fMRI and ECoG. Two months before electrode implantation, BOLD fMRI was used to localize visual areas. After implantation, a computed tomography (CT) scan was aligned to the pre-surgical structural MRI, with compensation for brain shift caused by implantation surgery (Hermes et al., 2010). Clinical analysis determined that the seizures did not originate near the reported electrode sites. After seizure recordings, the subject underwent a left anterior temporal lobectomy and amygdalohippocampotomy and remains seizure-free at almost 1 year of follow-up. The subject gave informed consent and this study was approved by the ethical committee of the University Medical Center Utrecht, in accordance with the Declaration of Helsinki 2008.

fMRI

Stimuli

Visual stimuli were presented by back-projection onto a 15.0 × 7.9 cm screen inside the MRI bore. The subject viewed the display through mirrors and the total distance from the subject's eyes (in the scanner) to the display screen was 41 cm. Display resolution was 1024 × 538 pixels. Stimuli were constrained to circular area filling the screen's vertical dimension, with any area outside this circle remaining at constant mean luminance. From the subject's point of view, this stimulus circle had a radius of 5.5° of visual angle.

The stimuli were generated in Matlab (MathWorks, Natick, MA, USA) using the PsychToolbox (Brainard, 1997; Pelli, 1997). They consisted of drifting bar apertures at various orientations that exposed a checkerboard pattern at 100% contrast (Dumoulin and Wandell, 2008). Alternating rows of checks moved parallel to the bar-orientation in opposite directions. The checkerboard motion direction reversed at random intervals, with a minimum of four seconds between reversals. The bar width subtended 1/4th of the stimulus radius (1.38°), and this was also the fundamental spatial frequency of the checkerboard. The contrast-defined bar moved across the stimulus aperture in 16 evenly spaced steps each 1/16th of the stimulus window diameter,

i.e. 0.69°. As there was one step at the start of each fMRI volume acquisition, each pass of the stimulus took 16 TRs, 24 seconds. Four bar orientations and two different motion directions for each bar were presented, giving a total of eight bar motion directions (upwards, downwards, left, right and four diagonals) within each scan. After each horizontal or vertical bar orientation pass, 12 seconds of mean-luminance (zero contrast) stimulus were displayed. As diagonal bar orientations were alternated with horizontal/vertical orientations, four mean-luminance blocks were presented at regular intervals during the scan.

The subject fixated a dot in the center of the visual stimulus. The fixation dot changed colors between red and green at random intervals. To ensure fixation was maintained subjects pressed a button on a response box every time the color changed, which was on average every 3 seconds, with a minimum change interval of 1.8 seconds. Performance on this task was consistently 97–100% correct.

MRI data acquisition

Anatomical MRI data were acquired on a Philips Achieva 3T scanner (Philips Medical Systems, Best, Netherlands) with a Quasar Dual gradient set. T1-weighted anatomical MRI data were acquired at an isotropic resolution of 1 mm³, with a field of view (FOV) of 288 × 288 × 175 mm. Repetition time (TR) was 9.958 ms, echo time (TE) was 4.59 ms, and flip angle was 8°. Functional T2*-weighted 2D echo planar images were acquired on a Phillips 7T scanner using a 16 channel head coil (Nova Medical, Wilmington, MA, USA) at a resolution of 2.06 × 2.06 × 2.3 mm, with an FOV of 230 × 175 × 85.1 mm. TR was 1500 ms, TE was 25 ms, and flip angle was 80°. Functional scans were each 168 time frames (252 seconds) in duration, of which the first eight time frames (12 seconds) were discarded to ensure the signal was at steady state. Three repeated scans were acquired within the same session.

Preprocessing of anatomical and functional images

fMRI analysis was performed in the mrVista software package for MATLAB, which is freely available at (<http://white.stanford.edu/software/>). T1-weighted anatomical scans were automatically segmented using FSL (Smith et al., 2004b) and then hand-edited to minimize segmentation errors (Teo et al., 1997) using ITK-SNAP (Yushkevich et al., 2006). The cortical surface was reconstructed at the gray-white matter border and rendered as a smoothed 3D surface (Wandell et al., 2000). Head movement and motion artifacts between and within functional scans were measured and corrected for Nestares and Heeger (2000). Functional data were then averaged across scans. Functional data were aligned to anatomical scans (Nestares and Heeger, 2000) and interpolated to the anatomical segmentation.

fMRI data-analysis

Population receptive field sizes and positions were estimated from the fMRI data and the visual stimulus position time course as described elsewhere (Dumoulin and Wandell, 2008). Briefly, the response of each recording site was predicted using a two-dimensional Difference of Gaussian (DoG) pRF model (Zuiderbaan et al., 2012). This modeled the center location (x and y parameters), the spread (σ_1) of the voxels' most responsive position to the stimulus, and the spread of the suppressive surround (σ_2). The predicted fMRI time course was calculated by convolution of the modeled pRF, the stimulus sequence and a fit BOLD hemodynamic response function (Harvey and Dumoulin, 2011). The pRF parameters for each voxel were determined by minimizing the sum of squared errors (RSS) between the predicted and observed fMRI time series.

The resulting visual field maps (pRF positions) were rendered onto an inflated cortical surface (Wandell et al., 2000), and the positions of visual field maps were determined and defined as regions of interest (ROIs) by relation to visual field representation (Sereno et al., 1995; Wandell et al., 2007).

ECoG

Stimuli

In ECoG recordings, stimuli were presented to the subject using a 15-inch LCD display (Samsung Syncmaster 214T, Seoul, Korea), measuring 30.5×22.9 cm, driven by a Toshiba Tecra S10-101 laptop (Toshiba, Tokyo, Japan). Display resolution was 1024×768 pixels. Viewed at a distance of 87 cm, the stimulus circle had a radius of 7.5°.

The visual stimuli were identical to the ones used in the fMRI experiment, except that the stimulus was 36% larger than that used in the fMRI experiment (7.5° radius versus 5.5°). Therefore, all visual angle measurements in this stimulus are 36% larger.

ECoG data acquisition

Arrays of ECoG electrodes (AdTech, Racine, WI, USA) were implanted subdurally for localization of seizure foci during the course of epilepsy treatment. These platinum electrodes had an interelectrode spacing of 1 cm and were 2.3 mm in diameter of exposed surface. One day after surgical electrode placement, a high resolution (0.5×0.5×1 mm) 3D CT scan was made to locate the electrodes (Philips Tomoscan SR 7000). The resulting electrode positions were projected to the nearest cortical surface point in the anatomical MRI (Hermes et al., 2010), which were then located relative to the visual field maps defined by fMRI analysis (Murphey et al., 2009). ECoG data were acquired with a 128 channel recording system (Micromed, Treviso, Italy) with 512 Hz sampling rate and 0.15–134.4 Hz band-pass filter. We localized two subdural electrodes to primary visual cortex (V1) and three electrodes to visual field maps along the medial side of the intraparietal sulcus (IPS2, two electrodes; IPS3, one electrode) (Fig. 1a). We elicited responses from these electrodes by showing the visual stimulus described above.

ECoG data analysis

Electrodes located in the occipital and parietal lobes were selected for analysis. The ECoG time-courses were re-referenced to the common average reference of all intracranial electrodes. A fast Fourier transform (FFT) notch filter was applied between 49 and 52 Hz to remove line noise around 50 Hz.

In line with the fMRI data and stimulus sequence, we divided the ECoG time-course into successive epochs of 1500 ms. Frequency components of each epoch of each electrode channel were determined using EEGLab (Delorme and Makeig, 2004). For each epoch, power spectral density (PSD) was determined at frequencies of 1 to 125 Hz in 0.1 Hz intervals. Epochs were divided into overlapping 500 ms time windows, whose signals were combined using Welch's averaged periodogram method (Welch, 1967), and a Hamming window to attenuate edge effects.

For most analyses, we grouped a range of frequencies together and determined the mean PSD in each epoch. However, the range of gamma frequencies (30–120 Hz) examined was very large, and the amplitude is very low at higher frequencies. As a result, the difference in amplitude would lead lower frequencies to dominate the mean signal. When we plotted the maximum amplitude at each frequency on a log-log axis, the amplitude was well fit by a straight line with a negative slope, as can be seen in Fig. 3b. A similar relationship has been reported in previous studies (Miller et al., 2009a, 2009b). We therefore normalized the amplitude at each frequency by this relationship, fit over data from all electrodes. Thus, the normalized amplitude was very similar at each frequency (Fig. 1b), which allowed us to average the data together over the entire gamma range with each frequency contributing similarly to the resulting signal.

This mean normalized PSD time course was then used to estimate the pRF properties, as described in for fMRI data. All V1 and IPS electrodes show increased 30–120 Hz power when the contrast-defined

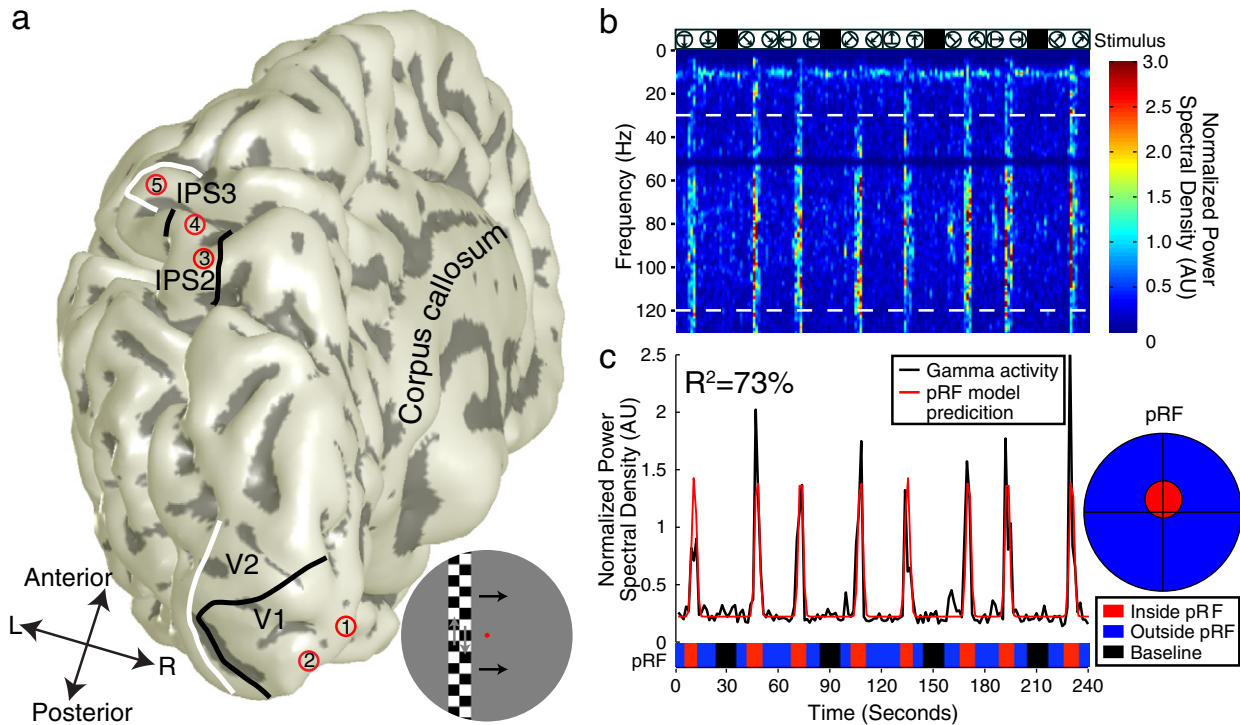


Fig. 1. Electrocorticographic pRF analysis. (a) Electrode locations on the left cortical surface. Inset shows a still frame from the contrast-defined bar stimulus, with gray arrows indicating the movement directions of the checks, and black arrows indicating the step direction of the bar. (b) Normalized power spectral density (PSD) across frequency and time for V1 electrode 1. Icons above indicate the stimulus sequence, showing different bar sweeps and mean luminance blocks (black). PSD amplitudes reveal the eight passes of the contrast-defined bar through the pRF. (c) Average PSD across 30–120 Hz (gamma) frequencies and corresponding pRF fit, shown by black and red lines, respectively. Epochs in which the stimulus fell within the pRF (two standard deviations) are shown along the bottom in red, stimulus positions outside the pRF are shown in blue and baseline stimulus presentation in black.

Table 1

Population receptive field properties for each electrode. These were determined from best fits of gamma range power time courses (Fig. 1C). fMRI-derived estimates of pRF size sigma are taken from the mean sigma at the same eccentricity as each ECoG electrode's preferred visual field location (X and Y parameters, relative to the fixation point) in the same visual field map in the same subject, given with the standard error of the mean, corrected for upsampling of fMRI data. This approach avoids uncertainty in visual field map positions of electrodes, which may be introduced by imperfect alignment of electrode positions with structural MRI scans. When interpreting comparisons between pRF size estimates from ECoG and fMRI in V1, it is important to remember that fMRI-derived estimates are influenced by the presence of a suppressive surround, while ECoG-derived estimates are not (Fig. 2).

Electrode	Area	X (°)	Y (°)	Sigma (°)	fMRI positive sigma (°) (SEM)	Variance explained
1	V1	0.15	−1.30	0.88	0.78 (0.20)	0.73
2	V1	0.25	−0.47	0.26	0.37 (0.17)	0.80
3	IPS2	1.22	0.04	1.54	3.08 (0.38)	0.40
4	IPS2	1.80	3.64	3.14	4.71 (1.15)	0.49
5	IPS3	0.90	0.52	1.76	2.96 (0.21)	0.36

bar was in a certain visual field position, allowing reliable estimates of pRF properties. For ECoG data, the predicted time course of the gamma frequency band mean power during each epoch was calculated by convolution of the modeled pRF and the stimulus sequence. Data and fits for a representative electrode are shown in Fig. 1c. The pRF properties measured were similar to those previously reported for fMRI and ECoG (Dumoulin and Wandell, 2008; Yoshor et al., 2007).

In a separate analysis (Fig. 3), we classified the epochs into three categories, as shown in Fig. 1c: those where the contrast-defined bar was inside the electrode's pRF, outside the pRF, or where no contrast-defined bar was shown (baseline). We defined epochs where the bar was inside an electrode's pRF when any part of the contrast-defined bar was within two standard deviations ($2\sigma_1$) of the pRF center. When a contrast-defined bar was shown, but this was not inside the pRF, the epoch was classified as stimulation outside the pRF. Epochs where no contrast-defined bar was shown (baseline) were determined from the stimulus sequence only. The power at each frequency for the mean epoch in each condition is shown in Figs. 3b and e. The results for the three conditions were compared using a general linear model to determine how well the response at each frequency band was predicted by each stimulus condition (Figs. 3c, f), with a sliding 3 Hz window of frequencies, centered at the frequency given on the x-axis.

When comparing oscillatory power between electrodes (Fig. 4) data were normalized based on the mean power during stimulation inside the pRF (taken as zero for alpha power and one for gamma power) and mean power during stimulation outside the pRF (taken as one for alpha power and zero for gamma power). Normalized alpha and gamma power in each epoch were compared using a paired t -test.

Results

In V1 and IPS gamma oscillations increase during visual stimulation of the preferred visual field locations

All V1 and IPS electrodes show increased 30–120 Hz power when the contrast-defined bar was in a certain visual field position, allowing reliable estimates of pRF properties, as described in the Methods. A representative pRF fit for a V1 electrode is shown in Fig. 1c. The pRF properties measured were similar to those previously reported for fMRI and ECoG (Dumoulin and Wandell, 2008; Yoshor et al., 2007), and are given in Table 1. In both V1 and IPS electrodes, power increased over this whole 30–120 Hz frequency range, with no clear peaks in power at specific frequencies (Figs. 1b, 3b, e). Such broadband changes in power have been reported before (Miller et al., 2009a, 2009b; Ray and Maunsell, 2011) and are referred to as broadband rather than gamma, acknowledging that different processes underlie broadband

power changes in the gamma range and changes at specific frequencies. We refer to this activity as gamma to denote this frequency range, though the changes in power here are clearly broadband in nature.

In V1 electrodes, this broadband range extended into the 3–7 Hz (theta) and 18–25 Hz (beta) bands. Therefore, theta, beta and gamma frequency ranges showed significantly increased activity when the pRF was stimulated, giving very similar responses (Figs. 3a–c). However, in IPS electrodes, PSD in the 3–25 Hz frequency range (theta, alpha and beta, Figs. 3d and e) significantly increased during baseline compared to stimulation either inside or outside the pRF (Figs. 3e and f). We also find increases in 3–25 Hz power during baseline in several other IPS electrodes whose gamma range power did not vary with stimulus position, i.e. in electrodes where no pRF could be fit. As such, theta and beta power are greatest during the baseline condition in IPS, but during stimulation within the pRF in V1. Alpha (9–12 Hz) power is also greatest during the baseline condition in IPS.

In V1 but not IPS alpha frequency oscillations increase during visual stimulation outside preferred visual field locations

Using fMRI, visual stimulation outside the pRF in early visual cortex decreases BOLD amplitudes below baseline, a negative BOLD response (Logothetis, 2002; Shmuel et al., 2006; Zuiderbaan et al., 2012). The addition of a surround to the pRF organization can capture these negative BOLD responses (Zuiderbaan et al., 2012). This is clear in fMRI responses at the sites where these electrodes were implanted, shown by the fit response profiles in Fig. 2. In the ECoG data (Fig. 1), however, gamma power in V1 electrodes never drops below baseline when the pRF's suppressive surround is stimulated. Consequently, we find no influence of surround suppression on pRF estimates derived from gamma activity (Fig. 2). This is true for all frequencies, except the narrow 9–12 Hz range (alpha oscillations, Figs. 3b and c).

To quantify these observations, we compared PSD over a broad range of frequencies during epochs when the contrast-defined bar was inside or outside the pRF or during baseline (Fig. 3c), using a general linear model (GLM) with the stimulus conditions (inside pRF, outside pRF and baseline recording) as regressors. Increases in alpha power were highly significantly predicted by the presence of the contrast-defined bar outside the pRF. The absence of a contrast-defined bar also predicted increased alpha power, though this effect was much less significant. At all other frequencies, stimulation inside the pRF predicted increases in power. We propose that this increase in alpha PSD during stimulation outside the pRF is elicited by stimulation of the suppressive surround. Surround stimulation in IPS electrodes predicts a slight increase in power in the gamma range, which reaches significance in some electrodes at some high frequencies. This may result from an imperfect description of the receptive field extent, particularly considering that pRFs fit from the IPS ECoG data are smaller than those from the fMRI data (Table 1, Fig. 2). We see no negative BOLD response with surround stimulation in fMRI of IPS visual field maps and, unlike in V1, no power increases at low frequencies.

V1 alpha oscillations are highly localized and depend on pRF and stimulus positions

If the changes in gamma and alpha power are associated with center and surround stimulation, they should reflect local processes and nearby cortical locations should show different responses depending on the local pRF properties. On the cortical surface the centers of the two electrodes within V1 were one centimeter apart whereas their visual field representations were partly overlapping. This configuration allowed us to examine responses when the contrast-defined bar was inside and outside both pRFs. These responses were used to normalize the gamma and alpha frequency responses (Figs. 4a and b).

In addition, this configuration allowed us to examine the several epochs where the contrast-defined bar fell inside one V1 electrode's

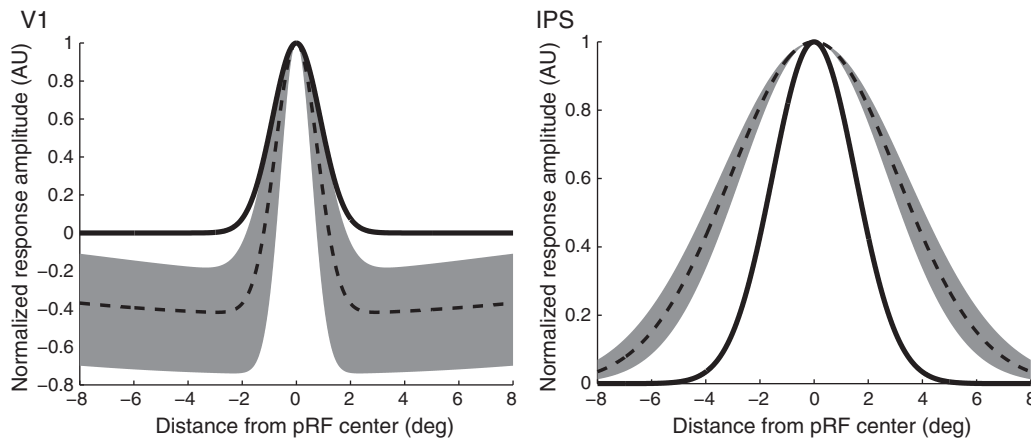


Fig. 2. Example profiles of pRFs derived from fMRI and ECoG recording sites in V1 and IPS2. While fit pRF properties from fMRI BOLD responses (dashed lines, standard error of the mean shown in gray, corrected for upsampling of fMRI data) show the influence of a suppressive surround, fits from gamma band activity (solid black lines, electrodes 1 and 3) show no such influence. PRF fits from gamma band ECoG data from IPS areas are consistently smaller than those seen from fMRI.

pRF, but outside the other, in its suppressive surround (Fig. 4c). If gamma and alpha frequency oscillations are related to the pRF's center-surround organization, this configuration should elicit different gamma and alpha frequency oscillations in the two electrodes.

During these epochs, in the electrode whose pRF surround was stimulated, alpha power was significantly higher and gamma power was significantly lower compared to the electrode whose pRF center was stimulated (Fig. 4d). As the gamma power was used to define the pRF, the gamma power dissociation is expected. However, at the same time and as predicted by stimulus position, there is also a clear dissociation in alpha power between nearby V1 locations (Fig. 4e). In addition, alpha power was not correlated between the two V1 electrodes either during stimulus presentation ($r = -0.03$) or baseline ($r = -0.04$), again demonstrating that alpha power is highly localized.

In the three IPS electrodes, on the other hand, alpha power was significantly correlated between any electrode combination during both stimulus presentation (minimum $r = 0.26$, maximum $p = 0.003$) and baseline (minimum $r = 0.39$, maximum $p = 0.027$). IPS theta power showed similar results, though correlations in beta power did not reach significance. Therefore, whereas V1 alpha power is localized during both stimulus presentation and baseline, IPS low-frequency power covaries between nearby locations, even if these locations are in different visual field maps within IPS.

Discussion

Summary

Local visual field stimulation increases broadband power at retinotopically corresponding sites in both V1 and IPS visual field maps. As broadband activity is not obscured by rhythmic oscillations that dominate the ECoG signal at lower frequencies, we are able to fit population receptive field (pRF) models in the 30–120 Hz range (gamma and high gamma). When stimulating outside these pRFs, 9–12 Hz power (alpha) increases at sites in V1, but not in IPS. This increase in alpha power is tightly localized: alpha power is uncorrelated between electrodes

separated by one centimeter and differs if the stimulus falls inside the pRF of one electrode (low alpha power) but outside the pRF of a nearby electrode (high alpha power). When no stimulus is shown, low frequency power increases at IPS sites over the whole 3–25 Hz range. Here, variations in low-frequency power are highly correlated between sites separated by over two centimeters. During this baseline condition a small alpha-specific power increase is seen in V1.

These results demonstrate that stimulation within the pRF leads to broadband increases in LFP power, associated with spiking activity (Manning et al., 2009; Whittingstall and Logothetis, 2009). Furthermore, V1 alpha oscillations reflect surround suppression, an active and computationally important process, and as such are tightly localized. When visual stimulation is absent, low frequency power increases, including alpha, in IPS suggest a large-scale suppression of activity.

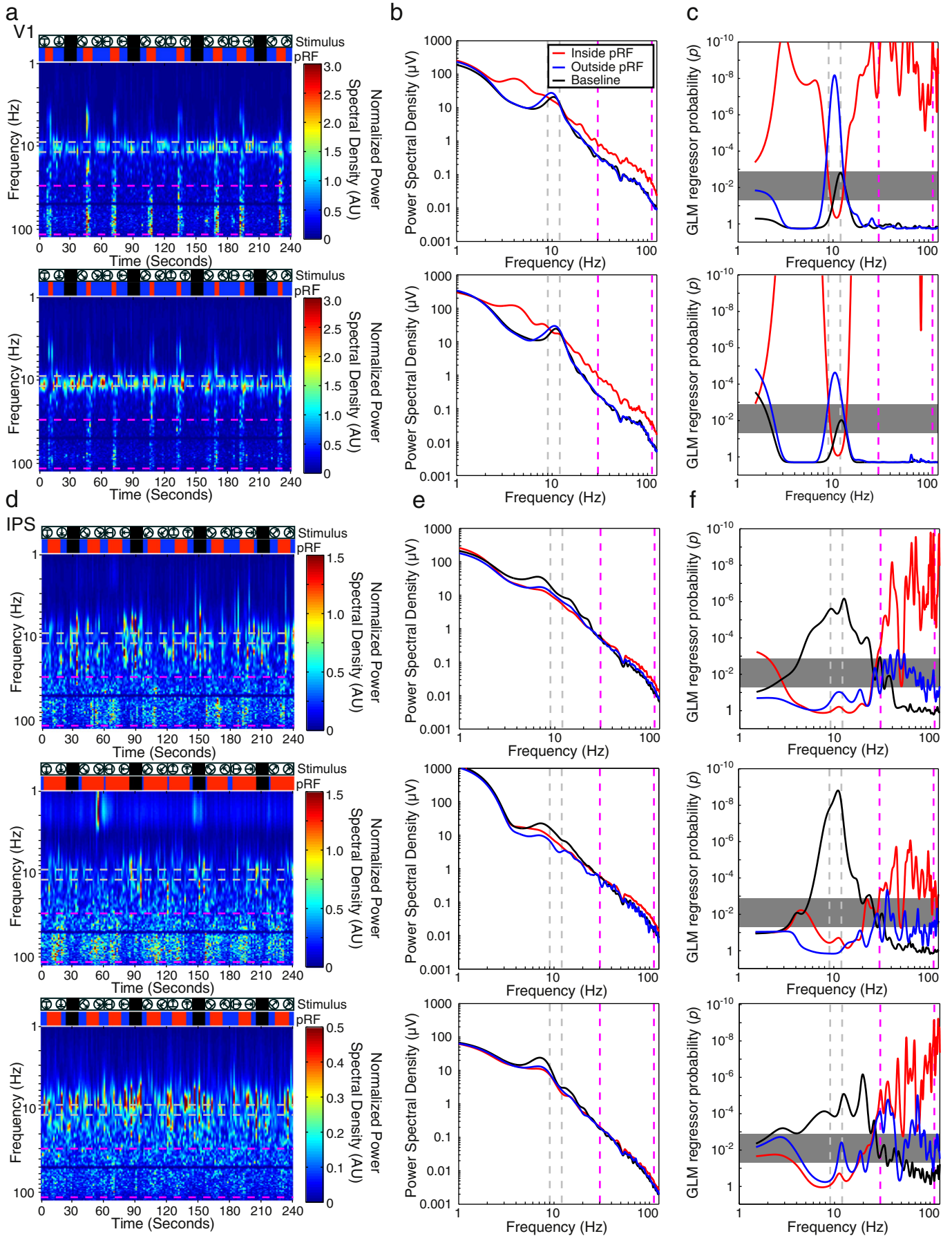
Role of alpha oscillations in resting and suppression

Two dominant functional roles are proposed to underlie alpha (9–12 Hz) oscillations. Both reflect suppression of broadband (spiking) activity. One idea suggests that alpha oscillations reflect functionally important processing at a local scale (Cooper et al., 2003, 2006; Jensen and Mazaheri, 2010; Palva et al., 2005a, 2005b), whereas the other idea proposes that alpha reflects disengagement of task-irrelevant areas at a larger spatial scale (Klimesch, 1996; Klimesch et al., 2007; Pfurtscheller, 2001, 2003; Ray and Cole, 1985). We find evidence for both proposals.

In V1, variations in alpha oscillation amplitudes are highly localized and vary as a function the stimulus position and the local pRF properties, in particular the surround. This strongly supports the former proposal in V1.

We also find evidence for the latter proposal. During baseline – resting – recording, we find an increase in power over the whole 3–25 Hz range in IPS, even in electrodes whose gamma range activity did not vary with stimulus position. Previous human ECoG work has also demonstrated that low-frequency oscillations in the absence of

Fig. 3. Spectral power changes when the stimulus is inside the pRF, outside the pRF, and during baseline. Each row represents one electrode, given in the order shown in Fig. 1a. In V1, stimulation inside the pRF (epochs labeled red) increases power over a broad frequency range (including gamma, magenta dashed lines), while stimulation outside the pRF (epochs labeled blue) increases power at 9–12 Hz (alpha, gray dashed lines) only. This is clear in the normalized spectrum (a) and when the spectrum is averaged across epochs with similar stimulation (b). Fitting each stimulus condition as a regressor in a GLM (c) shows that stimulation outside the pRF predicts increased power only around the alpha range. Stimulation inside the pRF predicts increased power at all frequencies except alpha. In IPS baseline presentation predicted increased power the whole 3–25 Hz range (d, e and f), while in the 30–120 Hz range stimulation inside the pRF predicted increased power (e and f). In the GLM fits (c and f) at each frequency, the top of the gray box indicates the alpha value for rejecting the null hypothesis after a conservative Bonferroni correction for multiple comparisons at different frequencies, while the bottom of the box indicates the uncorrected alpha level.



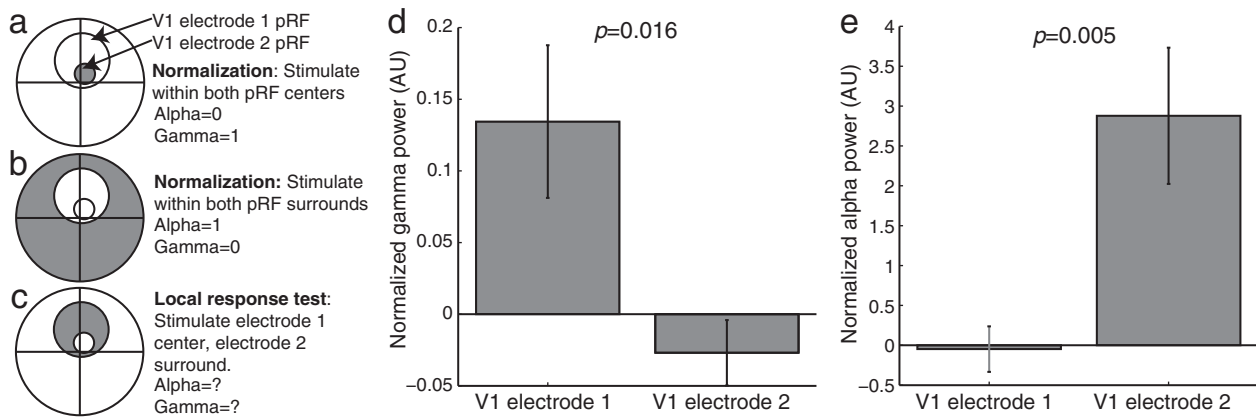


Fig. 4. V1 alpha oscillations induced by suppressive surround stimulation are highly localized, shown by comparison of normalized power from two electrodes one centimeter apart (Fig. 1a). a) Gamma power is high and alpha power is low in both electrodes when their common pRF center is stimulated. b) Alpha power is high and gamma is low when their common suppressive surround is stimulated. c) When the stimulus falls in the center of the pRF of electrode one but the surround of the pRF of electrode two, different responses would implicate a highly localized source of activity, with limited cortical spread. Similar responses would implicate effects acting at a larger scale. d) Gamma oscillations at neighboring electrodes differ when the stimulus activates their pRFs differently. However, pRFs were derived from gamma activity. e) Alpha oscillations are more powerful for the electrode whose pRF surround was stimulated, than for the electrode whose pRF center was stimulated. Differences were quantified using a two-sided paired *t*-test.

stimulation suppress broadband activity (Miller et al., 2010). In line with the idea of large-scale disengagement, we find that the time courses of low-frequency power changes are well correlated between recording sites separated by over two centimeters.

Also during baseline, in V1 we find a peak in oscillatory power specific to the alpha band. This peak in resting V1 alpha power only slightly exceeds the broadband power in the alpha range during pRF center stimulation. However, the frequency-specificity of this peak implicates some specific process, distinct from the broadband increase during stimulation within the pRF. Miller and colleagues suggest that principal component decomposition of the signal would reveal far higher alpha power in the baseline condition (Miller et al., 2009b). In line with this observation, others have shown an increase in low frequency oscillations during baseline in V1 using human brain mapping (Bartolo et al., 2011; Miller et al., 2010) and animal single unit recordings (Okun et al., 2010). Variations in alpha power during baseline recording in V1, unlike in IPS, are not correlated between nearby electrodes, implicating that the same local process generates alpha oscillations during surround stimulation.

Mechanism of suppression in V1

When the stimulus was shown in the surround, there was an increase in alpha power in V1, but no decrease in broadband activity below baseline. As such, there is no direct evidence of suppression of neural activity. In line with the very low baseline spiking activity in V1 (Hubel and Wiesel, 1959), we speculate that broadband activity is already at its minimum in the baseline condition. In line with previous studies (Carandini, 2004; Cavanaugh et al., 2002; Goldman et al., 2002; Goncalves et al., 2006; Miller et al., 2009b, 2010; Zuiderbaan et al., 2012), we interpret this increase in alpha power as the influence of a suppressive mechanism.

There are at least two plausible mechanisms by which surround suppression might lead to an increase in alpha frequencies. First, GABAergic interneurons have been implicated in V1 surround suppression (Fitzpatrick, 2000) and alpha oscillations (Crunelli and Leresche, 1991; Jones et al., 2000; Lopes da Silva et al., 1976; Marshall et al., 2002). The highly local nature of these alpha oscillations implicates intra-cortical connections and/or tightly localized cortico-cortical connections in surround suppression (Schwabe et al., 2006, 2010). Second, recent work in cats suggests that surround suppression may result from decreased non-thalamic excitatory drive rather than increased inhibition (Ozeki et al., 2009). Here the authors suggest that V1 must operate as an inhibition-stabilized network in which excitatory recurrence

destabilizes visual responses. This non-inhibitory origin of surround suppression is also a good candidate for the mechanism involved here.

We speculate that the V1 alpha oscillations reflect subthreshold changes in membrane potential of the underlying neural population. Electrophysiological measurements of spiking activity typically report that surround suppression modulates the spiking activity of neurons only when the classical receptive field is stimulated at the same time (Carandini, 2004; Cavanaugh et al., 2002; Fitzpatrick, 2000). Analogous to spiking rates, this interaction of the stimulated receptive field with its suppressive surround seems to produce a modulation of gamma-band oscillations (Gieselmann and Thiele, 2008; Ray and Maunsell, 2011). However, stimulating the surround alone does not decrease spiking rates, most likely due to the low baseline firing rate of neurons in primary visual cortex. Because of this lack of effect on spiking activity without classical receptive field stimulation, surround suppression is often referred to as “extraclassical” and “silent.” Unlike spiking activity, fMRI BOLD signals have significant baseline activity, and decrease below baseline when only stimulating the surround (Zuiderbaan et al., 2012) and may also be driven more by changes in membrane potential rather than spiking rates (Logothetis et al., 2001). Alpha oscillations provide an electrophysiological signature of this “silent” suppression.

Surround suppression is modulated by attention (Muller and Kleinschmidt, 2004). We did not attempt to manipulate our subject's attention, except giving a simple task at fixation. As such, it is possible that this attentional modulation of surround suppression affects our measurements.

Links between ECoG with fMRI signals

Our results link broadband ECoG oscillations to increases in BOLD responses, and alpha oscillations to decreases (negative) in BOLD responses. Both observations are in line with previous studies.

In all electrodes broadband power in the gamma range allows reliable pRF estimates comparable to previous measurements using fMRI (Dumoulin and Wandell, 2008; Harvey and Dumoulin, 2011; Yoshor et al., 2007). Similar pRF estimates support the finding that increases in BOLD responses are correlated with gamma activity in EEG (Mukamel et al., 2005; Niessing et al., 2005). Broadband power at beta and theta frequencies also allowed similar pRF estimates in V1 but not in IPS. This difference seems to be because the power of rhythmic oscillations during baseline recording in IPS exceeds the increase in broadband power in during stimulation inside the pRF (Miller et al., 2009b). Recent studies suggest that spiking activity generates these broadband power changes (Manning et al., 2009;

Whittingstall and Logothetis, 2009). This relationship suggests that the broadband power increase we see during stimulation inside the pRF results from an increase in spike rate, which should be evident at the scale of ECoG recordings (Miller, 2010; Okun et al., 2010).

These observations also link ECoG alpha oscillations to negative BOLD, in line with the observations that negative BOLD responses are correlated with alpha activity (Goldman et al., 2002; Gonçalves et al., 2006; Mukamel et al., 2005; Scheeringa et al., 2009). Notably, like spiking activity but unlike the BOLD response, broadband power in V1 electrodes never drops below baseline when only the pRF's suppressive surround is stimulated, consistent with reports of local field potentials in macaque V1 (Gieselmann and Thiele, 2008).

Conclusion

This study demonstrates a link between alpha oscillations and surround suppression in V1. These alpha oscillations are highly localized. This provides a clear role for alpha oscillations in local neural computations.

These alpha oscillations suppress broadband (spiking) activity. The same suppressive mechanism also seems to be involved in producing negative (below baseline) BOLD responses in V1.

Low-frequency oscillations in IPS visual field maps also increase during baseline recording, which also seems to be involved in suppression of broadband (spiking) activity. However, the time courses of these oscillations are highly correlated over large areas of the cortical surface, implicating a larger-scale mechanism than operates in V1, and consistent with a role of alpha as a large-scale inhibitor of task-irrelevant areas. This contrasts with the role in local computations in V1. These results suggest that alpha oscillations can be involved in distinct functional roles, but these both involve suppressive mechanisms.

Acknowledgments

This work was supported by NWO Vidi grant no. 452.08.008, a Focus and Massa initiative grant from Neuroscience and Cognition Utrecht, Utrecht University grant UGT7685, and grants from STW (Netherlands Technology Foundation), NWO applied science division, and the Technology Program of the Netherlands Ministry of Economic Affairs. We wish to thank Dr. D. Hermes for her help with data collection.

References

- Bartolo, M.J., Gieselmann, M.A., Vuksanovic, V., Hunter, D., Sun, L., Chen, X., Delicato, L.S., Thiele, A., 2011. Stimulus-induced dissociation of neuronal firing rates and local field potential gamma power and its relationship to the resonance blood oxygen level-dependent signal in macaque primary visual cortex. *Eur. J. Neurosci.* 34, 1857–1870.
- Brainard, D.H., 1997. The psychophysics toolbox. *Spat. Vis.* 10, 433–436.
- Carandini, M., 2004. Receptive fields and suppressive fields in the early visual system. In: Gazzaniga, M.S. (Ed.), *The Cognitive Neurosciences*. MIT Press, Cambridge, MA, pp. 312–326.
- Cavanaugh, J.R., Bair, W., Movshon, J.A., 2002. Nature and interaction of signals from the receptive field center and surround in macaque V1 neurons. *J. Neurophysiol.* 88, 2530–2546.
- Cooper, N.R., Croft, R.J., Dominey, S.J., Burgess, A.P., Gruzeliel, J.H., 2003. Paradox lost? Exploring the role of alpha oscillations during externally vs. internally directed attention and the implications for idling and inhibition hypotheses. *Int. J. Psychophysiol.* 47, 65–74.
- Cooper, N.R., Burgess, A.P., Croft, R.J., Gruzeliel, J.H., 2006. Investigating evoked and induced electroencephalogram activity in task-related alpha power increases during an internally directed attention task. *Neuroreport* 17, 205–208.
- Crunelli, V., Leresche, N., 1991. A role for GABAB receptors in excitation and inhibition of thalamocortical cells. *Trends Neurosci.* 14, 16–21.
- Delorme, A., Makeig, S., 2004. EEGLAB: an open source toolbox for analysis of single-trial EEG dynamics including independent component analysis. *J. Neurosci. Methods* 134, 9–21.
- Dumoulin, S.O., Wandell, B.A., 2008. Population receptive field estimates in human visual cortex. *Neuroimage* 39, 647–660.
- Ermentrout, G.B., Kopell, N., 1998. Fine structure of neural spiking and synchronization in the presence of conduction delays. *Proc. Natl. Acad. Sci. U. S. A.* 95, 1259–1264.
- Fitzpatrick, D., 2000. Seeing beyond the receptive field in primary visual cortex. *Curr. Opin. Neurobiol.* 10, 438–443.
- Gieselmann, M.A., Thiele, A., 2008. Comparison of spatial integration and surround suppression characteristics in spiking activity and the local field potential in macaque V1. *Eur. J. Neurosci.* 28, 447–459.
- Goldman, R.I., Stern, J.M., Engel Jr., J., Cohen, M.S., 2002. Simultaneous EEG and fMRI of the alpha rhythm. *Neuroreport* 13, 2487–2492.
- Goncalves, S.L., de Munck, J.C., Pouwels, P.J., Schoonhoven, R., Kuijter, J.P., Maurits, N.M., Hoogduin, J.M., Van Someren, E.J., Heethaar, R.M., Lopes da Silva, F.H., 2006. Correlating the alpha rhythm to BOLD using simultaneous EEG/fMRI: inter-subject variability. *Neuroimage* 30, 203–213.
- Harvey, B.M., Dumoulin, S.O., 2011. The relationship between cortical magnification factor and population receptive field size in human visual cortex: constancies in cortical architecture. *J. Neurosci.* 31, 13604–13612.
- Hermes, D., Miller, K.J., Noordmans, H.J., Vansteensel, M.J., Ramsey, N.F., 2010. Automated electrocorticographic electrode localization on individually rendered brain surfaces. *J. Neurosci. Methods* 185, 293–298.
- Hubel, D.H., Wiesel, T.N., 1959. Receptive fields of single neurones in the cat's striate cortex. *J. Physiol.* 148, 574–591.
- Jensen, O., Mazaheri, A., 2010. Shaping functional architecture by oscillatory alpha activity: gating by inhibition. *Front. Hum. Neurosci.* 4, 186.
- Jones, S.R., Pinto, D.J., Kaper, T.J., Kopell, N., 2000. Alpha-frequency rhythms desynchronize over long cortical distances: a modeling study. *J. Comput. Neurosci.* 9, 271–291.
- Klimesch, W., 1996. Memory processes, brain oscillations and EEG synchronization. *Int. J. Psychophysiol.* 24, 61–100.
- Klimesch, W., Sauseng, P., Hanslmayr, S., 2007. EEG alpha oscillations: the inhibition-timing hypothesis. *Brain Res. Rev.* 53, 63–88.
- Kopell, N., Ermentrout, G.B., Whittington, M.A., Traub, R.D., 2000. Gamma rhythms and beta rhythms have different synchronization properties. *Proc. Natl. Acad. Sci. U. S. A.* 97, 1867–1872.
- Logothetis, N.K., 2002. The neural basis of the blood-oxygen-level-dependent functional magnetic resonance imaging signal. *Philos. Trans. R. Soc. Lond. B Biol. Sci.* 357, 1003–1037.
- Logothetis, N.K., Pauls, J., Augath, M., Trinath, T., Oeltermann, A., 2001. Neurophysiological investigation of the basis of the fMRI signal. *Nature* 412, 150–157.
- Lopes da Silva, F.H., van Rotterdam, A., Barts, P., van Heusden, E., Burr, W., 1976. Models of neuronal populations: the basic mechanisms of rhythmicity. *Prog. Brain Res.* 45, 281–308.
- Manning, J.R., Jacobs, J., Fried, I., Kahana, M.J., 2009. Broadband shifts in local field potential power spectra are correlated with single-neuron spiking in humans. *J. Neurosci.* 29, 13613–13620.
- Marshall, L., Henze, D.A., Hirase, H., Leinekugel, X., Dragoi, G., Buzsáki, G., 2002. Hippocampal pyramidal cell-interneuron spike transmission is frequency dependent and responsible for place modulation of interneuron discharge. *J. Neurosci.* 22, RC197.
- Miller, K.J., 2010. Broadband spectral change: evidence for a macroscale correlate of population firing rate? *J. Neurosci.* 30, 6477–6479.
- Miller, K.J., Sorensen, L.B., Ojemann, J.G., den Nijs, M., 2009a. Power-law scaling in the brain surface electric potential. *PLoS Comput. Biol.* 5, e1000609.
- Miller, K.J., Zanos, S., Fetz, E.E., den Nijs, M., Ojemann, J.G., 2009b. Decoupling the cortical power spectrum reveals real-time representation of individual finger movements in humans. *J. Neurosci.* 29, 3132–3137.
- Miller, K.J., Hermes, D., Honey, C.J., Sharma, M., Rao, R.P., den Nijs, M., Fetz, E.E., Sejnowski, T.J., Hebb, A.O., Ojemann, J.G., Makeig, S., Leuthardt, E.C., 2010. Dynamic modulation of local population activity by rhythm phase in human occipital cortex during a visual search task. *Front. Hum. Neurosci.* 4, 197.
- Mukamel, R., Gelbard, H., Arieli, A., Hasson, U., Fried, I., Malach, R., 2005. Coupling between neuronal firing, field potentials, and fMRI in human auditory cortex. *Science* 309, 951–954.
- Muller, N.G., Kleinschmidt, A., 2004. The attentional 'spotlight's' penumbra: center-surround modulation in striate cortex. *Neuroreport* 15, 977–980.
- Murphy, D.K., Maunsell, J.H., Beauchamp, M.S., Yeshor, D., 2009. Perceiving electrical stimulation of identified human visual areas. *Proc. Natl. Acad. Sci. U. S. A.* 106, 5389–5393.
- Nestares, O., Heeger, D.J., 2000. Robust multiresolution alignment of MRI brain volumes. *Magn. Reson. Med.* 43, 705–715.
- Niessing, J., Ebisch, B., Schmidt, K.E., Niessing, M., Singer, W., Galuske, R.A., 2005. Hemodynamic signals correlate tightly with synchronized gamma oscillations. *Science* 309, 948–951.
- Okun, M., Naim, A., Lampl, I., 2010. The subthreshold relation between cortical local field potential and neuronal firing unveiled by intracellular recordings in awake rats. *J. Neurosci.* 30, 4440–4448.
- Ozeki, H., Finn, I.M., Schaffer, E.S., Miller, K.D., Ferster, D., 2009. Inhibitory stabilization of the cortical network underlies visual surround suppression. *Neuron* 62, 578–592.
- Palva, J.M., Palva, S., Kaila, K., 2005a. Phase synchrony among neuronal oscillations in the human cortex. *J. Neurosci.* 25, 3962–3972.
- Palva, S., Linkenkaer-Hansen, K., Naatanen, R., Palva, J.M., 2005b. Early neural correlates of conscious somatosensory perception. *J. Neurosci.* 25, 5248–5258.
- Pelli, D.G., 1997. The VideoToolbox software for visual psychophysics: transforming numbers into movies. *Spat. Vis.* 10, 437–442.
- Pfurtscheller, G., 2001. Functional brain imaging based on ERD/ERS. *Vision Res.* 41, 1257–1260.
- Pfurtscheller, G., 2003. Induced oscillations in the alpha band: functional meaning. *Epilepsia* 44 (Suppl. 12), 2–8.
- Ray, W.J., Cole, H.W., 1985. EEG alpha activity reflects attentional demands, and beta activity reflects emotional and cognitive processes. *Science* 228, 750–752.
- Ray, S., Maunsell, J.H., 2011. Different origins of gamma rhythm and high-gamma activity in macaque visual cortex. *PLoS Biol.* 9, e1000610.
- Scheeringa, R., Petersson, K.M., Oostenveld, R., Norris, D.G., Hagoort, P., Bastiaansen, M.C., 2009. Trial-by-trial coupling between EEG and BOLD identifies networks

- related to alpha and theta EEG power increases during working memory maintenance. *Neuroimage* 44, 1224–1238.
- Schwabe, L., Obermayer, K., Angelucci, A., Bressloff, P.C., 2006. The role of feedback in shaping the extra-classical receptive field of cortical neurons: a recurrent network model. *J. Neurosci.* 26, 9117–9129.
- Schwabe, L., Ichida, J.M., Shushruth, S., Mangapathy, P., Angelucci, A., 2010. Contrast-dependence of surround suppression in Macaque V1: experimental testing of a recurrent network model. *Neuroimage* 52, 777–792.
- Sereno, M.I., Dale, A.M., Reppas, J.B., Kwong, K.K., Belliveau, J.W., Brady, T.J., Rosen, B.R., Tootell, R.B., 1995. Borders of multiple visual areas in humans revealed by functional magnetic resonance imaging. *Science* 268, 889–893.
- Shmuel, A., Augath, M., Oeltermann, A., Logothetis, N.K., 2006. Negative functional MRI response correlates with decreases in neuronal activity in monkey visual area V1. *Nat. Neurosci.* 9, 569–577.
- Smith, A.T., Williams, A.L., Singh, K.D., 2004a. Negative BOLD in the visual cortex: evidence against blood stealing. *Hum. Brain Mapp.* 21, 213–220.
- Smith, S.M., Jenkinson, M., Woolrich, M.W., Beckmann, C.F., Behrens, T.E., Johansen-Berg, H., Bannister, P.R., De Luca, M., Drobnjak, I., Flitney, D.E., Niazy, R.K., Saunders, J., Vickers, J., Zhang, Y., De Stefano, N., Brady, J.M., Matthews, P.M., 2004b. Advances in functional and structural MR image analysis and implementation as FSL. *Neuroimage* 23 (Suppl. 1), S208–S219.
- Tajima, S., Watanabe, M., Imai, C., Ueno, K., Asamizuya, T., Sun, P., Tanaka, K., Cheng, K., 2010. Opposing effects of contextual surround in human early visual cortex revealed by functional magnetic resonance imaging with continuously modulated visual stimuli. *J. Neurosci.* 30, 3264–3270.
- Teo, P.C., Sapiro, G., Wandell, B.A., 1997. Creating connected representations of cortical gray matter for functional MRI visualization. *IEEE Trans. Med. Imaging* 16, 852–863.
- Traub, R.D., Whittington, M.A., Stanford, I.M., Jefferys, J.G., 1996. A mechanism for generation of long-range synchronous fast oscillations in the cortex. *Nature* 383, 621–624.
- Wandell, B.A., Chial, S., Backus, B.T., 2000. Visualization and measurement of the cortical surface. *J. Cogn. Neurosci.* 12, 739–752.
- Wandell, B.A., Dumoulin, S.O., Brewer, A.A., 2007. Visual field maps in human cortex. *Neuron* 56, 366–383.
- Welch, P., 1967. The use of fast Fourier transform for the estimation of power spectra: a method based on time averaging over short, modified periodograms. *IEEE Trans. Audio Electroacoust.* 15, 70–73.
- Whittingstall, K., Logothetis, N.K., 2009. Frequency-band coupling in surface EEG reflects spiking activity in monkey visual cortex. *Neuron* 64, 281–289.
- Williams, A.L., Singh, K.D., Smith, A.T., 2003. Surround modulation measured with functional MRI in the human visual cortex. *J. Neurophysiol.* 89, 525–533.
- Yoshor, D., Bosking, W.H., Ghose, G.M., Maunsell, J.H., 2007. Receptive fields in human visual cortex mapped with surface electrodes. *Cereb. Cortex* 17, 2293–2302.
- Yushkevich, P.A., Piven, J., Hazlett, H.C., Smith, R.G., Ho, S., Gee, J.C., Gerig, G., 2006. User-guided 3D active contour segmentation of anatomical structures: significantly improved efficiency and reliability. *Neuroimage* 31, 1116–1128.
- Zenger-Landolt, B., Heeger, D.J., 2003. Response suppression in v1 agrees with psychophysics of surround masking. *J. Neurosci.* 23, 6884–6893.
- Zuiderbaan, W., Harvey, B.M., Dumoulin, S.O., 2012. Modeling center-surround configurations in population receptive fields using fMRI. *J. Vis.* 12 (3), 10.